were 14.4 cm and 10.5 cm for the oblique anterior beam and 11.8 cm and 10.5 cm for the oblique posterior beam.

In Fig. 1a, two peaks were apparent around 0% and 6–8% for the IC dose. The first peak corresponded to the tumor located beside the mediastinum where the lung region was not largely included in the main beam path, and the second peak corresponded to the tumor isolated in the lung region where the beam path largely included the lung region. The average differences between the physical and effective depth were 0.1 cm for the first peak (from –1 to 1%) and 3.1 cm for the second peak (from 6 to 8%). In the latter case, the inhomogeneity effect was greater. For the same reason, the boost plan was more affected by the inhomogeneity correction than the first plan. The average differences increased from 4% (first plan) to 6% (boost plan).

This retrospective study showed that the actual delivered doses were an overdose, to some extent, with respect to the IC dose. However, we cannot recommend a general increase of the prescription dose when applying the inhomogeneity correction, because there were some cases that showed the opposite results. For the first plan of Case 20, the difference in the IC dose was –3%. The IC dose increased if the inhomogeneity correction was applied. Differences between the physical depth and the effective depth were 12.1 cm and 11.9 cm, respectively, for the anterior beam and 9.2 cm and 10.0 cm, respectively, for the posterior beam. The effective depth was larger than the physical depth for the posterior beam. In this case, the tumor was beside the mediastinum. The D_{95} dose prescription has been considered to be a superior method in such a case. D_{95} expresses the dose coverage of the PTV so that local control of the tumor has a strong relationship with this value. We showed the same retrospective data for D_{95} of PTV2 on Fig. 1a and 1b. The differences in D_{95} were 1% average and –9% (Case 4) maximum for the first plan (1a) and 1% average and –6% (Case 4) maximum for the boost plan (1b). The deviations were less than the IC dose. However, there were some cases that show differences over 5%. From the point of view of maintaining the treatment outcome, careful consideration of the D_{95} prescription is necessary.

Frank *et al.*[12] compared three plans: one plan was generated by the traditional homogeneous point-dose prescription, a second plan was generated by the traditional method with the inhomogeneity correction, and a third plan was generated by the inhomogeneity-corrected volume-dose prescription that would cover 95% of the PTV. Their conclusion was that inhomogeneity-corrected methods produce an equivalent PTV, clinical target volume (CTV), and IC doses while providing superior PTV coverage. Each institution should perform such a retrospective consideration.

Regarding the PTVp, the mean dose that corresponded to the overdosage of the uncorrected plan was systematically large. However, the D_{95} showed a Gaussian distribution in which the center value was close to 0%. In some cases, like the isolated tumor in the lung region, the dose at the border of the tumor decreased because of a re-build up effect. Only a model-based algorithm could consider such effects. Unintended hot spots or cold spots can be detected retrospectively by analyzing the Dmax and Dmin. Differences of more than 10% were observed for both parameters. The differences for Dmin were notably large. Cases with severe underdosage must have occured. We added the homogeneity index (HI) analysis, which is the ratio between Dmax and Dmin within the PTVp. The differences in HI between the corrected and uncorrected plans showed an increase in average value from 1.21 to 1.31 for the first plan and from 2.39 to 2.45 for the boost plan.

Regarding PTVn, mean doses showed a similar high tendency; however, D_{95} was also high compared with the PTVp data. The lymph node is generally beside the mediastinum so that the re-buildup effect seemed small. The deviations were relatively less than those for the PTVp, but some cases had differences in excess of 10%.

By using a model-based algorithm, the delivered dose to the lung increased as the expansion of dose kernel. On the other hand, V_{20} analysis integrated the delivered dose of the whole lung region. As a result, differences were not observed. The spinal code also showed no meaningful difference. (Table 3) A possible explanation is that for the first AP field irradiation, the field includes a large part of the spinal code and the tumor tends to be beside the mediastinum so that the major part of the beam axis is not in the lung region. Therefore, the difference between the physical depth and the effective depth is small. For the boost oblique field irradiation, the cord is normally shielded.

In conclusion, we carried out a retrospective analysis of lung cancer between inhomogeneity corrected and uncorrected conditions of 25 patients among five institutions of radiation therapy. IC dose and the D_{95} of PTV2 were analyzed in order to consider prescription validity. D_{95} prescription seemed to be a superior method; however, its reliability depends on each clinical case. Additionally, D_{95}, Dmax, Dmin and Dmean for the PTVp and PTVn were analyzed and found that the target volume had accepted unintended underdose more than 10% for the worst case. Finally, an analysis for the organ at risk was added. There were no apparent differences for the V_{20} of the lung and the Dmax of the spinal code. These results provide a standard for the effects of the inhomogeneity correction.

ACKNOWLEDGEMENTS

This work was supported by Japan Society of Medical Physics (JSMP) research group, task group 02 and also by The Japanese College of Medical Physics. We thanks to the member of task group 02 for their valuable advice. We also acknowledge all the staff of the five institutions of radiation therapy for helping with the retrospective analysis.

REFERENCES

1. American Association of Physicists in Medicine; Report of Task Group No. 65 (2004) Tissue Inhomogeneity Corrections for Megavoltage Photon Beams. AAPM report 85.
2. Mah K and Van Dyk J (1991) On the impact of tissue inhomogeneity corrections in clinical thoracic radiation therapy. Int J Radiat Oncol Biol Phys **21**: 1257–1267.
3. Tada T, *et al* (2002) Inhomogeneity Correction in Radiotherapy for Lung Cancer in Multicenter Clinical Trials. Radiat Med **20**(4): 191–194.
4. Papanikolaou N, Klein EE and Hendee WR (2000) Heterogeneity corrections should be used in treatment planning for lung cancer? Med Phys **27**(8): 1702–1704.
5. Butts JR and Foster AE (2001) Comparison of commercially available three-dimensional treatment planning algorithms for monitor unit calculations in the presence of heterogeneities. J Appl Clin Med Phys Winter **2**(1): 32–41.
6. Radiation Therapy Oncology Group (1991) A Phase III Study of Radiation Therapy Alone or in Combination with Chemotherapy for Patients with Non-Small Cell Lung Cancer RTOG 88-08.
7. Hasenbalg F, *et al* (2007) Collapsed cone convolution and analytical anisotropic algorithm dose calculations compared to VMC++ Monte Carlo simulations in clinical cases. Phys Med Biol **52**(13): 3679–3691.
8. Xiao Y, *et al* (2009) Dosimetric evaluation of heterogeneity corrections for RTOG 0236: stereotactic body radiotherapy of inoperable stage I-II non-small-cell lung cancer. Int J Radiat Oncol Biol Phys **73**(4): 1235–1242.
9. Ding GX, *et al* (2007) Impact of inhomogeneity corrections on dose coverage in the treatment of lung cancer using stereotactic body radiation therapy. Med Phys **34**(7): 2985–2994.
10. Matsuo Y, *et al* (2007) Interinstitutional variations in planning for stereotactic body radiation therapy for lung cancer. Int J Radiat Oncol Biol Phys **68**(2): 416–425.
11. JASTRO treatment planning guideline 2008 (http://www.kkr-smc.com/rad/guideline/2008/).
12. Frank SJ, *et al* (2003) Treatment planning for lung cancer: traditional homogeneous point-dose prescription compared with heterogeneity-corrected dose-volume prescription. Int J Radiat Oncol Biol Phys **56**(5): 1308–1318.

Received on May 26, 2010
Revision received on October 13, 2010
Accepted on October 28, 2010
J-STAGE Advance Publication Date: December 24, 2010

Int. J. Radiation Oncology Biol. Phys., Vol. 79, No. 5, pp. 1479–1486, 2011

0360-3016/$–see front matter

ELSEVIER

doi:10.1016/j.ijrobp.2009.12.048

CLINICAL INVESTIGATION **Liver**

DOSE–VOLUME HISTOGRAM ANALYSIS OF THE SAFETY OF PROTON BEAM THERAPY FOR UNRESECTABLE HEPATOCELLULAR CARCINOMA

MITSUHIKO KAWASHIMA, M.D.,*† RYOSUKE KOHNO, PH.D.,* KOHEI NAKACHI, M.D.,‡ TEIJI NISHIO, PH.D.,* SHUICHI MITSUNAGA, M.D.,‡ MASAFUMI IKEDA, M.D.,‡ MASARU KONISHI, M.D.,§ SHINICHIRO TAKAHASHI, M.D.,§ NAOTO GOTOHDA, M.D.,§ SATOKO ARAHIRA, M.D.,† SADAMOTO ZENDA, M.D.,* TAKASHI OGINO, M.D.,* AND TAIRA KINOSHITA, M.D.§

Divisions of *Particle Therapy and Radiation Oncology, Research Center for Innovative Oncology, †Radiation Oncology, ‡Hepatobiliary and Pancreatic Medical Oncology, and §Hepatobiliary and Pancreatic Surgery, National Cancer Center Hospital East, Kashiwa, Japan

Purpose: To evaluate the safety and efficacy of radiotherapy using proton beam (PRT) for unresectable hepatocellular carcinoma.

Methods and Materials: Sixty consecutive patients who underwent PRT between May 1999 and July 2007 were analyzed. There were 42 males and 18 females, with a median age of 70 years (48–92 years). All but 1 patient had a single lesion with a median diameter of 45 mm (20–100 mm). Total PRT dose/fractionation was 76–cobalt Gray equivalent (CGE)/20 fractions in 46 patients, 65 CGE/26 fractions in 11 patients, and 60 CGE/10 fractions in 3 patients. The risk of developing proton-induced hepatic insufficiency (PHI) was estimated using dose-volume histograms and an indocyanine-green retention rate at 15 minutes (ICG R15).

Results: None of the 20 patients with ICG R15 of less than 20% developed PHI, whereas 6 of 8 patients with ICG R15 values of 50% or higher developed PHI. Among 32 patients whose ICG R15 ranged from 20% to 49.9%, PHI was observed only in patients who had received 30 CGE (V30) to more than 25% of the noncancerous parts of the liver ($n = 5$) Local progression-free and overall survival rates at 3 years were 90% (95% confidence interval [CI], 80–99%) and 56% (95% CI, 43–69%), respectively. A gastrointestinal toxicity of Grade ≥2 was observed in 3 patients.

Conclusions: ICG R15 and V30 are recommended as useful predictors for the risk of developing PHI, which should be incorporated into multidisciplinary treatment plans for patients with this disease. © **2011 Elsevier Inc.**

Hepatocellular carcinoma, Proton beam radiotherapy, Dose–volume histogram, Radiation tolerance of the liver.

INTRODUCTION

Recent improvements in diagnostic imaging and radiotherapy (RT) techniques have made high-dose radiotherapy a safe and effective treatment for selected patients with unresectable hepatocellular carcinoma (HCC) (1). Charged-particle radiotherapy can potentially deliver considerably larger doses of RT to liver tumors, with greater sparing of normal tissues, and proton beam radiotherapy (PRT) for HCC using aggressively high total and fractional RT doses has been investigated during the last 2 decades. The results have shown local control rates ranging from 75% to 96% and overall survival (OAS) rates exceeding 50% at 2 years in groups of patients that include those who had HCC tumors of ≥5 cm in diameter (2–4). HCC has a high propensity for venous invasion, which is frequently associated with multiple tumors within resected specimens (5–9). In this context, the extent of resection was determined while considering potential tumor spread via portal blood flow and the necessity of preserving a functional liver reserve (5, 7, 10). Even in preselected patients who underwent hepatectomy, more than 50% of tumors with diameters greater than 4 cm demonstrated microscopic vascular invasion (8, 11). Consequently, it will become more crucial to consider the influence of vascular invasion on undetectable tumor dissemination at the periphery of the gross tumor in RT for unresectable HCC.

Given the high probability of obtaining local control by using PRT, an appropriate definition of the clinical target volume (CTV) according to patterns of tumor spread and patients' functional liver reserves is extremely important in order to maximize the therapeutic ratio. Ideally, the entire portal segment that contains HCC nodules should be covered within the CTV when the tumor shows macro- or microscopic vascular invasion. This requires a considerably larger

Reprint requests to: Mitsuhiko Kawashima, 6-5-1, Kashiwanoha, Kashiwa, Chiba, Japan, 277-8577. Tel: 81-4-7133-1111; Fax: 81-4-7171-4724; E-mail: mkawashi@east.ncc.go.jp

Conflict of interest: none.

Received Nov 24, 2009, and in revised form Dec 21, 2009. Accepted for publication Dec 21, 2009.

irradiated volume even with PRT, partly because of unavoidable uncertainty in treatment planning without using intraoperative ultrasonography (7). Another possible way to eradicate satellite HCC nodules, which are disseminated via portal blood flow, is transarterial chemoembolization (TACE). Currently, the standard treatment for patients with unresectable HCC that is not amenable to local ablation therapy is TACE instead of best supportive care (12). The OAS rate at 3 years after TACE ranges from 32% to 47% in patients with stage III cancer and with liver damage A to B, according to the staging system used in a nationwide cohort study conducted by the Liver Cancer Study Group of Japan (13). Considering that the tumoricidal effect of TACE in HCC with vascular invasion is frequently incomplete (13), a significant benefit of adding PRT to TACE would be expected. However, presently, there has been no robust evidence supporting this concept. Before we examine the validity of targeting the entire anatomical portal segment containing HCC in a multidisciplinary approach that includes PRT, practical methods to estimate the safety of PRT according to the dose–volume histogram (DVH) should be established in patients who have various levels of severity of liver dysfunction. Findings from our previous study consisting of 30 patients suggested that the risk of proton-induced hepatic insufficiency (PHI) could be predicted by the indocyanine green clearance test and the retention rate at 15 minutes (ICG R15) in combination with DVH parameters (14) such as percentages of hepatic noncancerous portions receiving doses of >30 cobalt-Gray-equivalent (CGE) (3). We have subsequently accumulated data from additional patients in clinical practice. The clinical results were evaluated, and we have again used the DVH analysis to examine the relationship between probability of PHI and dose–volume parameters.

METHODS AND MATERIALS

Patients

Patient eligibility was reported previously (3); in brief, they were required to have uni- or bidimensional measurable HCC nodules of ≤10 cm in maximum diameter on computed tomography (CT) and/or magnetic resonance imaging (MRI) without evidence of extrahepatic tumor spread. All patients had a white blood cell count of ≥2,000/mm^3; a hemoglobin level of ≥7.5 g/dl; a platelet count of ≥25,000/ mm^3; and adequate hepatic function (total bilirubin, ≤3.0 mg/dl; alkaline phosphatase, aspartate aminotransferase, and alanine aminotransferase of <5.0× normal; no ascites). Patients who had multicentric HCC nodules were not considered as candidates for PRT, except for those who fulfilled the following two conditions: (*1*) multiple nodules could be encompassed within a single clinical target volume; and (*2*) lesions other than those of the targeted tumor were judged to be controlled with prior surgery and/or local ablation therapy. This retrospective study was approved by the institutional ethics committee, and written informed consent was obtained from all patients.

Treatment Planning

ICG R15 was measured in all patients to quantitatively assess the hepatic functional reserve. Serological testing for hepatitis B surface antigen and anti-hepatitis C antibody was done. All patients were judged to be unresectable by expert hepatobiliary surgeons at our institution, based on the patient's serum bilirubin level, ICG R15, and expected volume of resected liver (10). Percutaneous fine-needle biopsies were performed for all patients unless they had radiologically compatible, postsurgical recurrent HCC (3).

Treatment methods were published previously (3). In brief, gross tumor volume (GTV) was defined using a treatment-planning CT scan, and CTV and planning target volume (PTV) were defined as follows in all but 2 patients: CTV = GTV + 5 mm, and PTV = CTV + 3 mm of lateral, craniocaudal, and anteroposterior margins. CTV encompassed the entire volume of the right lobe in 1 patient who had a tumor of 4 cm in diameter that broadly attached to the bifurcation of the right anterior and posterior portal veins. In this patient, right portal vein embolization was done to facilitate compensatory hypertrophy of the left lobe for expected surgery. However, the patient was finally judged to be unresectable, and PRT was selected. Another patient was treated with a CTV encompassing the entire right anterior portal segment because a tumor of 2 cm in diameter had invaded the bifurcation of the right anterosuperior and anteroinferior portal vein associating with daughter HCC at the right anterosuperior portal segment. The beam energy and spread-out Bragg peak (15) were fine-tuned so that a 90% isodose volume of the prescribed dose encompassed the PTV.

Forty-six patients received PRT to a total dose of 76 CGE in 3.8 CGE once-daily fractions, four to five fractions in a week. Another 3 patients underwent 60 CGE /10 fractions/2 weeks, depending on availability of the proton beam. Eleven patients whose PTV encompassed the gastrointestinal wall received 65 CGE in 2.5 CGE /fraction, five fractions per week. All patients were treated using a 150- to 190-MV proton beam. The relative biological effectiveness of our proton beam was defined as 1.1 (16). No concomitant treatment such as TACE, local ablation, or systemic therapy was allowed during or after the PRT, unless a treatment failure was detected. Both scanning of CT images for treatment planning and irradiation by the proton beam were done during the exhalation phase using the respiration-gated irradiation system and intrahepatic fiducial markers as previously reported (3).

Outcomes

Death from any cause was defined as an event in calculation of OAS, whereas tumor recurrences at any site or patient deaths were defined as events in disease-free survival (DFS). An increase of the tumor diameter within the PTV was defined as local progression, and patients who died without evidence of local progression were censored at the time of last radiographic examination. Adverse events were reviewed weekly during the PRT regimen by means of physical examination, complete blood count, liver function tests, and other biochemical profiles as indicated. The severity of adverse events was assessed using the National Cancer Institute common terminology criteria for adverse events, version 3.0. After completion of PRT, reviews that monitored disease status, including CT and/or MRI examinations and long-term toxicity, were done at a minimum frequency of every 3 months in all 60 patients. The percentages of hepatic noncancerous portions (entire liver volume minus gross tumor volume) receiving CGE doses of >0 (V0), ≥10 (V10), ≥20 (V20), ≥30 (V30), ≥40 (V40), and ≥50 (V50) were calculated using PRT planning software (PT-PLAN/NDOSE System, Sumitomo Heavy Industries Ltd., Tokyo, Japan), and their influence on the outcomes were analyzed (3). Time-to-event analyses were done using Kaplan-Meier estimates from the start of PRT. The differences between time-to-event curves were evaluated with the log-rank test. Multivariate analyses were performed with Cox's proportional hazards model.

RESULTS

Patients

A total of 60 patients with HCC underwent PRT in our institution between May 1999 and July 2007. Approximately 1400 patients with HCC were newly presented to our institution during this study period and about 35%, 30%, 25%, and the remainder primarily treated with hepatectomy, TACE, percutaneous local ablation, and other treatments, respectively. Therefore 60 patients in this study corresponded to approximately 4% of overall, or 7% of patients with unresectable HCC. Patient characteristics at the start of PRT are listed in Table 1. All patients had underlying chronic liver disease. One patient had a history of schistosomiasis, and another patient had autoimmune hepatitis as the cause of liver cirrhosis. Five additional patients were diagnosed with liver cirrhosis caused by non-B, non-C hepatitis. A total of 24 patients received PRT as the first treatment for their HCC. Ten patients had postsurgical recurrences, 22 patients received unsuccessful local ablation and/or TACE to the targeted tumor, and 4 patients underwent successful local ablation to a tumor other than the target prior to PRT. Histological confirmation was not obtained in 1 patient who had a tumor with typical radiographic features compatible with HCC (3). Six patients had HCC nodules of ≤3 cm in diameter; however, they were not considered candidates for local ablation therapy because of the tumor locations, which were in close proximity to the great vessels or the lung.

Table 1. Characteristics of patients

Characteristics	No. of patients (%)
Age (years)	
Median	70
Range	48–92
Gender	
Male	42 (70)
Female	18 (30)
ECOG performance status	
0–1	57 (95)
2	3 (5)
Viral markers	
Hepatitis B surface antigen-positive	3 (5)
Hepatitis C antibody-positive	49 (82)
Both positive	1 (2)
Both negative	7 (12)
Child-Pugh classification	
A	47 (78)
B	13 (22)
C	0
% patients with pretreatment ICG R15 values	
<20	20 (20)
20–40	25 (55)
40–50	7 (12)
≥50	8 (13)
Tumor size (mm)	
Median	45
Range	20–90
20–50	42 (70)
>50	18 (30)
Macroscopic vascular invasion	
Yes	42 (70)
No	18 (30)
Morphology of primary tumor	
Single nodular	45 (75)
Multinodular, aggregating	9 (15)
Diffuse	5 (8)
Portal vein tumor thrombosis	1 (2)
Serum alpha-fetoprotein level (IU/mL)	
<300	41 (68)
≥300	19 (32)
Histology	
Well-differentiated	15 (25)
Moderately-differentiated	28 (47)
Poorly-differentiated	7 (12)
Differentiation not specified	9 (15)
Negative (radiological diagnosis only)	1 (2)
Prior treatment	
None	24 (40)
Surgery	10 (17)
Local ablation/TACE	26 (43)

Adverse events during PRT

All patients completed the treatment plan. Prolongation of the overall treatment time for more than 1 week occurred in 4 patients: treatment of 3 patients was extended due to availability of the proton beam machine, and 1 patient's treatment was extended because of fever associated with grade 3 elevation of total bilirubin that spontaneously resolved within a week. A total of 14 patients experienced transient grade 3 leukopenia and/or thrombocytopenia without infection or bleeding that necessitated treatment. In addition, 8 patients experiencing grade 3 elevation of transaminases without clinical manifestation of hepatic insufficiency maintained good performance status. PRT was not discontinued for these patients; nevertheless, these events spontaneously resolved within 1 to 2 weeks.

Estimation of the risk of PHI by DVH analysis

Development of hepatic insufficiency presented with anicteric ascites and/or asterixis within 6 months after completion of PRT in the absence of disease progression was defined as PHI. Eleven patients, all of whom received a total PRT dose of 76 CGE, developed PHI at 1 to 6 months (median, 2 months) after completion of PRT without elevation of serum bilirubin and transaminases of more than threefold above normal levels. DVHs for hepatic noncancerous portions were drawn according to pretreatment ICG R15 values (Fig. 1A–C). Results showed that all 20 patients with ICG R15 of <20% were free of PHI, regardless of the DVH, for 2 to 94 months (median, 44 months). On the other hand, 6 of 8 patients with pretreatment ICG R15 values of ≥50% died of PHI with (n = 3) or without (n = 3) evidence of HCC recurrence at 2 to 15 months (median, 8 months). There was no obvious relationship between DVH and development of PHI in these 8 patients, as shown in Fig. 1C.

Among 32 patients whose ICG R15 values ranged from 20% to 49.9%, 5 patients developed PHI. The V0 to V50 in these 32 patients are shown in Fig. 2. Differences in distributions of these DVH parameters between patients who did

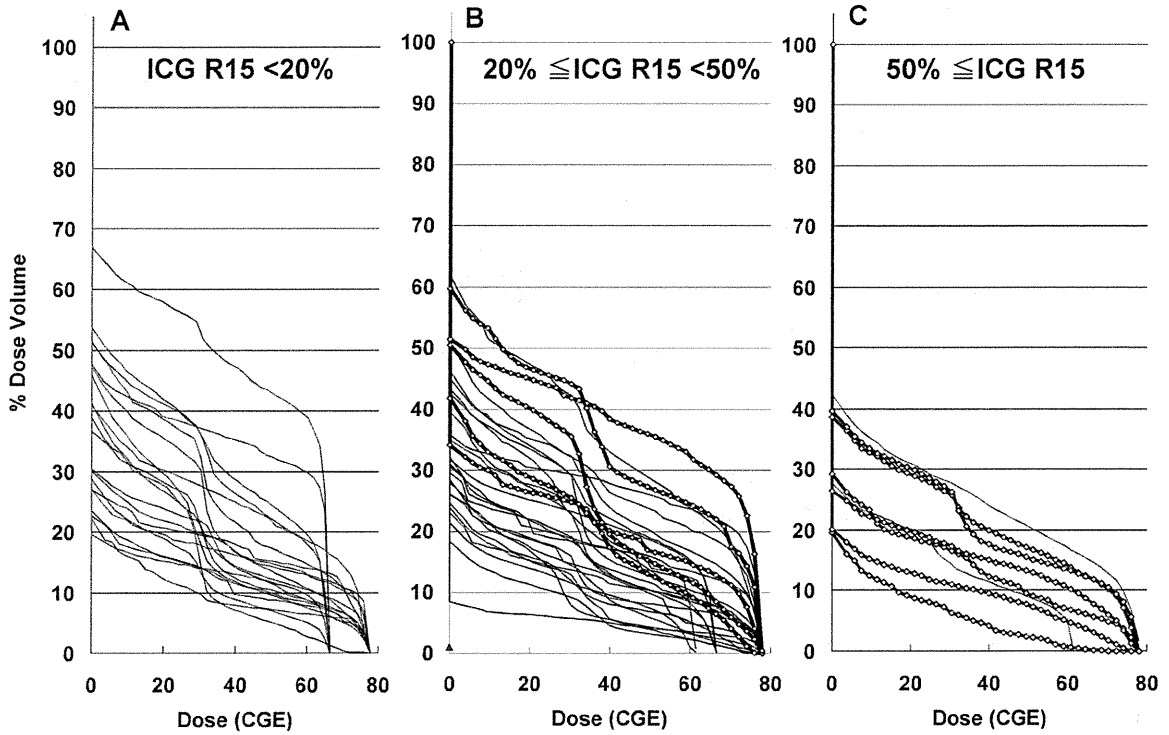

Fig. 1. DVH are shown for all patients according to their pretreatment ICG R15 values, as noted in each panel. Thick lines with rhomboid symbols represent DVHs for patients suffering from hepatic insufficiency within 6 months after completion of PRT.

and did not develop PHI were statistically significant, with p values of 0.012 in V0, 0.009 in V10, 0.012 in V20, 0.006 in V30, 0.016 in V40, and 0.024 in V50 (Mann-Whitney U test). The lowest p value was observed in the difference at V30. Among 32 patients whose ICG R15 values ranged from 20% to 49.9%, none of the 21 patients whose V30 were <25% experienced PHI, whereas 5 of 11 patients (45%) whose V30 was ≥25% developed PHI (p = 0.037, Mann-Whitney U test). The incidence of PHI was 2/25 (8%) in Child-Pugh class A patients, whereas PHI incidence was 3/7 (43%) in class B patients in this group of 32 patients (p = 0.218, Mann-Whitney U test). Of 5 patients who experienced PHI, 1 died at 8 months without evidence of HCC recurrence. PHI spontaneously resolved in 4 patients; 2 patients died of intrahepatic recurrence at 22 and 71 months, respectively; 1 patient died of brain metastasis at 8 months; and 1 patient was alive and disease free at 50 months. In both of the patients who survived for more than 4 years despite development of PHI, the pretreatment functional liver reserve was Child-Pugh class A and ICG R15 was less than 40%. On the other hand, all 3 patients who experienced PHI and died within 2 years had Child-Pugh class B liver functions. Relationships between ICG R15 and V30 according to occurrence of PHI in Child-Pugh class A and B patients are shown in Fig. 3a and b, respectively.

Other serious adverse events

Three patients experienced a gastrointestinal toxicity grade of ≥2. One patient developed hemorrhagic duodenitis associated with anemia at 2 months after completion of 76 CGE/20 fractions/30 days of PRT. The dose administered to the duodenum was estimated to be 50 to 80% of the prescribed dose. Bypass surgery was attempted to alleviate the symptoms; however, this patient died of postoperative hepatic failure at 6 months. Two patients received 65 CGE/26 fractions of PRT, with the entire circumference of the gastrointestinal walls covered within the PTV. One of these 2 patients experienced grade 3 hemorrhagic ulcer at the ascending colon, within the PTV. The patient was managed successfully with right hemicolectomy at 10 months; however, the patient

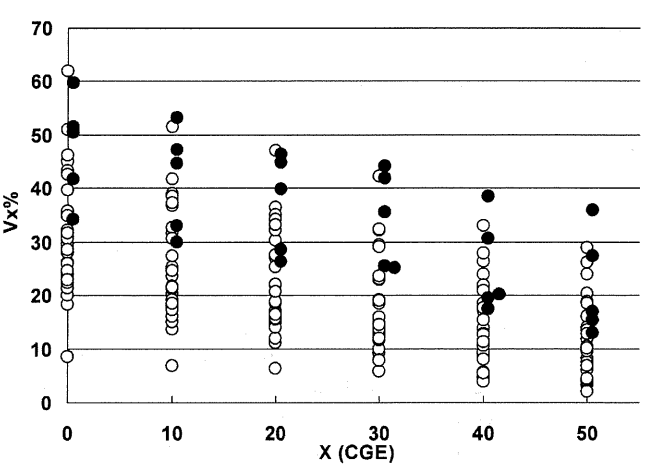

Fig. 2. Distribution of V0 to V50 in DVHs for 32 patients whose pretreatment ICG R15 values ranged from 20% to 49.9%. Open circles represent values for patients who did not experience PHI, whereas closed circles represent those who developed PHI.

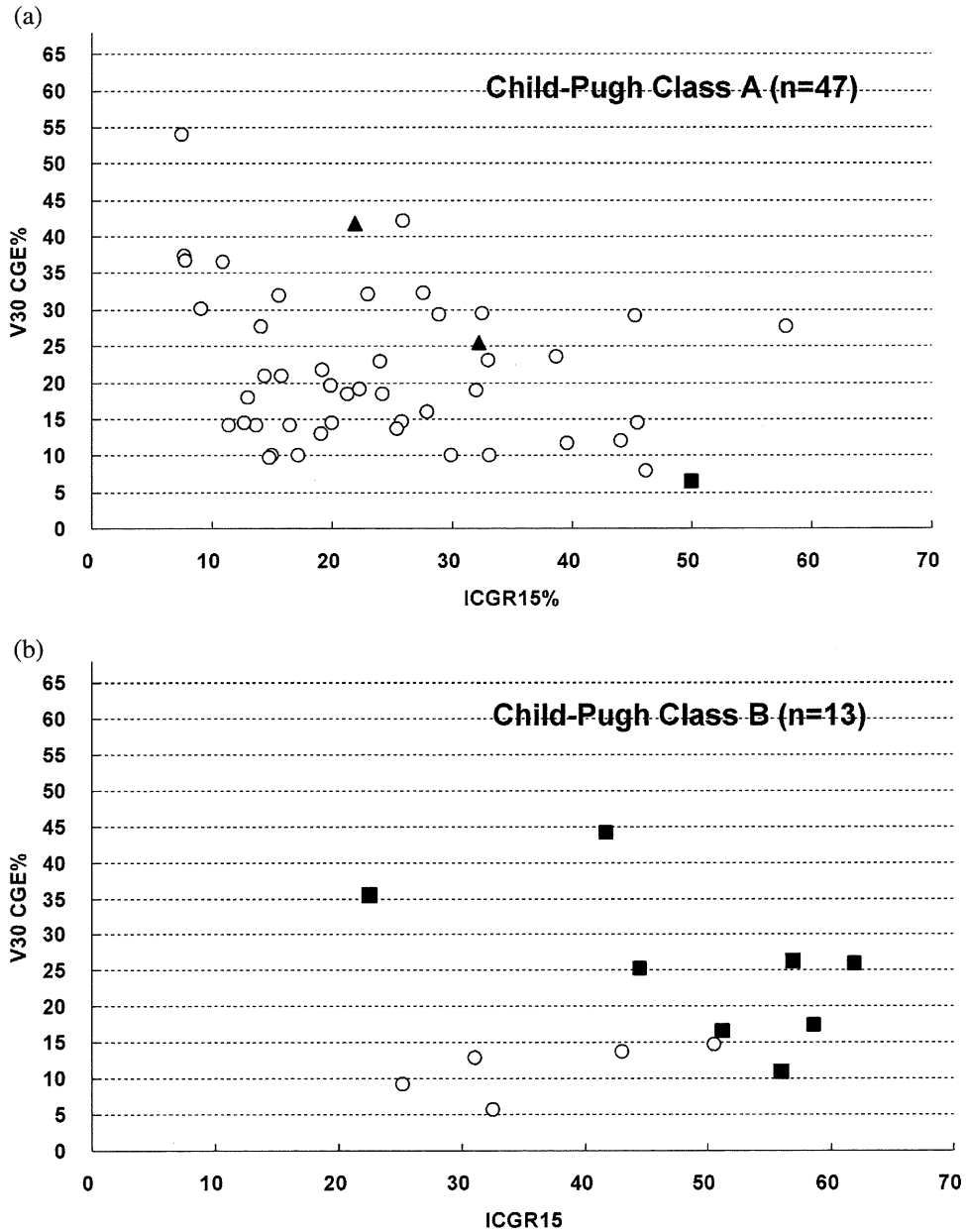

Fig. 3. Scattergram of V30 in each patient who had pretreatment liver functions classified as Child-Pugh class A (a) and class B (b), as shown in each panel, according to the ICG R15 value. Open circles represent values in patients who did not experience PHI. Closed squares represent those who developed PHI and died within 2 years with ($n = 5$) or without ($n = 4$) disease recurrence. Closed triangles represent those who experienced transient PHI and survived for more than 4 years after commencement of PRT.

died of local recurrence and subsequent hepatic failure at 23 months. The other patient developed grade 2 esophagitis within the PTV at 7 months. Repetitive balloon dilatations were required to alleviate the patient's dysphagia; however, the patient was alive without disease and taking a normal diet at 30 months. There were no other observations made of adverse events of Grade ≥3 in any of the patients.

Tumor control and survival

At the time of analysis in August 2009, 42 patients had already died because of intrahepatic recurrence in 27, nodal recurrence in 1, distant metastasis in 3, hepatic insufficiency without recurrence in 9, comorbidity in 1, and senility in 1. Forty of these 42 patients had been free from local progression until death; the durations ranged from 2 to 77 months (median, 20 months). Two patients who experienced local progression died subsequently. A total of 15 patients were alive at 25 to 92 months (median, 43 months) without local progression. Three patients were alive at 49, 53, and 94 months, respectively, after salvage treatment for local progression, using local ablation in 2 and TACE in 1 A total of 37 patients achieved complete disappearance of the primary tumor at 1 to 50 months (median, 10 months) post-PRT. Eighteen patients had residual tumor masses on CT

and/or MRI for 2 to 44 months (median, 21 months) until the time of death or last follow-up visit without local progression. The local progression-free (LPF) rates at 3 and 5 years were 90% (95% confidence interval [CI], 80%–99%) and 86% (95% CI, 74%–98%), respectively.

Of 5 patients who experienced local progression, 3 patients underwent 65 CGE/26 fractions, and 2 patients received 76 CGE/20 fractions of PRT. All 3 patients who received 60 CGE/10 fractions were free from local progression at 6, 30, and 51 months, respectively. LPF rates at 3 and 5 years for 46 patients who received 76 CGE/20 fractions were 97% (95% CI, 92%–100%) and 93% (95% CI, 83%–100%), respectively. LPF rates at 3 years for 11 patients who underwent 65 CGE/26 fractions of PRT were 56% (95% CI, 16%–95%) and was worse than that in patients who received 76 CGE/20 fractions with statistical significance ($p = 0.005$).

A total of 32 patients developed intrahepatic tumor recurrences that were outside of the PTV at 1 to 62 months (median, 20 months). Nine of these tumors occurred within the same segment of the primary tumor. Nodal recurrence at the hepatoduodenal ligament and distant metastasis were observed as the first sites of failure in 2 and 3 patients, respectively. In addition to the above-mentioned five deaths from PHI or postsurgical mortality, 4 patients died of hepatic failure because of underlying liver disease at 17 to 23 months, and 2 patients died from other reasons (comorbidity or senility) without evidence of HCC recurrence. Seven patients remained alive and disease free at 27 to 51 months (median, 30 months). The median survival time for all 60 patients was 41 months, and actuarial OAS rates at 3 and 5 years were 56% (95% CI, 43%–69%) and 25% (12%–39%), respectively. DFS rates at 3 and 5 years were 18% (95% CI, 7%–29%) and 4% (95% CI, 0%–12%), respectively, as shown in Fig. 4. Two Child-Pugh class A patients who underwent PRT with the CTV covering the entire right lobe or right anterior portal segment were alive and disease free at 50 and 26 months, respectively. The former patient had a pre-PRT ICG R15 of 22% and received a V30 of 42% and experienced transient PHI that resolved spontaneously; the latter patient, whose corresponding parameters were 8% and 37%, respectively, did not experience PHI.

Factor analysis

Univariate analyses revealed that factors related to functional liver reserve and occurrence of PHI had significant influence on OAS ($p < 0.05$). Liver function (Child-Pugh class A or B) and prior treatment (none or recurrent) were independent and significant prognostic factors ($p < 0.002$), and occurrence of PHI had marginal significance ($p = 0.011$) by multivariate analysis, as shown in Table 2. The DFS rate at 3 years for 24 patients who had no prior treatment for HCC was 35% (95% CI, 14%–56%), whereas DFS for the remaining 36 patients was 7% (95% CI, 0%–17%) ($p = 0.011$). In Child-Pugh class A patients, OAS at 3 and 5 years for those who had no prior treatment ($n = 17$) was 76% (95% CI, 56%–97%) and 59% (95% CI, 33%–86%), respectively, and 63% (95% CI, 45%–80%) and 25% (95% CI, 7%–42%), respectively, for 30 patients with recurrent tumor ($p = 0.060$). In Child-Pugh class B patients, the 2-year OAS for patients without PHI ($n = 5$) was 80% (95% CI, 45%–100%), while 8 patients who developed PHI died within 2 years with ($n = 5$) or without ($n = 3$) HCC recurrence ($p = 0.009$).

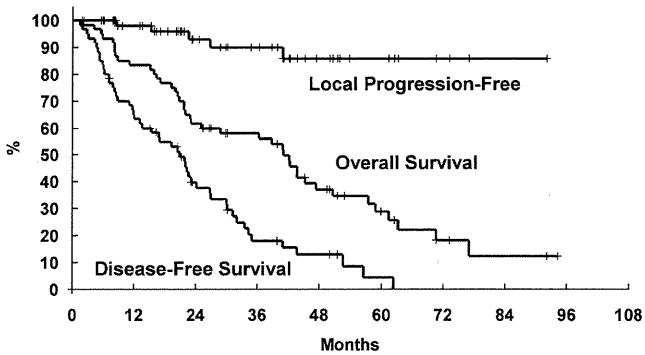

Fig. 4. Kaplan-Meier estimation of local progression-free survival, OAS, and disease-free survival rates for all 60 patients.

DISCUSSION

The promising tumoricidal effect of PRT using aggressive escalation of total and fractional doses, which has been repeatedly reported previously, was reproduced in this study (3, 4). The estimated actuarial local progression-free rate within the PTV in patients receiving 76 CGE/20 fractions exceeded 90% at 3 years. DFS at 3 years for patients who underwent PRT as an initial treatment ($n = 24$) was 35%, and, among them, OAS at 3 years was 76% in Child-Pugh class A patients ($n = 17$). These results are comparable to those observed after surgical treatment (17). Although the number of patients was small, these data indicate that appropriate local control with PRT may provide survival benefit in adequately selected patients with unresectable HCC. The fact that 9 of the 32 intrahepatic HCC recurrences occurred within the same anatomical portal segments showed that it should still be possible to improve the progression-free rate by defining the CTV so it covers undetectable tumor spread via the portal blood flow.

As shown in Fig. 3, no patient who had ICG R15 of less than 20% experienced PHI. In addition, only Child-Pugh class A patients with pre-PRT ICG R15 of less than 40% survived for longer than 4 years despite development of PHI. One of them underwent systematic portal segmental irradiation with the CTV covering the entire right lobe, and the details for this patient will be reported separately. On the other hand, all patients who had pre-PRT liver functions classified as Child-Pugh class B and/or ICG R15 of 40% or higher died within 2 years when they developed PHI. This suggests that the role of systematic portal irradiation requiring a large irradiated volume should be pursued further in Child-Pugh class A patients with favorable ICG R15 values; otherwise, the CTV should be confined to the GTV with adequate margins. Furthermore, in patients who have ICG R15 of 50% or

Table 2. Factors related to overall survival

Factor	No. of patients	% of OAS at 3 years (MST, months)	Univariate *p* value	Multivariate *p* value, hazard ratio (95% CI)
Age				
<70	29	55 (41)	0.660	0.087
≥70	31	61 (42)		0.52 (0.24–1.10)
Gender				
Male	42	62 (41)	0.332	0.194
Female	18	44 (42)		0.62 (0.29–1.30)
Tumor size (mm)				
<50	36	66 (44)	0.178	0.070
≥50	24	46 (23)		0.54 (0.28–1.05)
Pretreatment ICG R15				
<40%	45	67 (44)	0.002	
≥40%	15	33 (15)		
Child-Pugh classification				
A	47	68 (45)	<0.001	<0.001
B	13	23 (15)		0.19 (0.07–0.50)
Serum alfa-fetoprotein level (IU/mL)				
<300	41	61 (42)	0.617	0.618
≥300	19	53 (39)		0.83 (0.39–1.74)
PHI				
No	49	65 (44)	0.001	0.011
Yes	11	18 (9)		0.29 (0.11–0.76)
% of patients receiving V30				
<25%	40	57	0.724	
≥25%	20	60		
Total dose = 65 Gy				
Yes	11	44 (29)	0.646	0.185
No	49	61 (42)		1.88 (0.73–4.76)
Prior treatment				
None	24	67 (47)	0.112	0.002
Recurrence	36	53 (36)		0.32 (0.15–0.66)

Abbreviations: OAS = overall survival; MST = median survival time; CI = confidence interval; PHI = proton-induced hepatic insufficiency.

higher, the indication for PRT should be considered with extreme caution to prevent life-threatening PHI, as shown in Fig. 3.

Results of this retrospective study showed 56% OAS at 3 years in all patients and 68% in 47 Child-Pugh class A patients. All of them were judged strictly as unresectable and not amenable to local ablation. Therefore, a survival benefit of adding PRT to TACE could be expected, which should be tested in randomized trials. Suitable candidates for such a study may be patients who have unresectable HCC of >4 cm in diameter (*i.e.*, a high probability of microscopic vascular invasion) or who show macroscopic vascular invasion, which is amenable to selective segmental TACE as a curative treatment. Nevertheless, before developing that kind of randomized study, data should still be compiled regarding the safety and patterns of failure after PRT combined with TACE while ICG R15 and V30 are taken into account. Preliminary results of hypofractionated stereotactic body radiotherapy for patients with relatively small primary or metastatic liver tumors showed 70% to >90% of objective response rates and 20 or more months of median survival time (1, 18–20). Mature data regarding the relationship between oncological outcomes and tumor characteristics, as well as functional reserve of the liver, are needed to optimize cost-effectiveness of localized, high-dose RT using X-ray or charged particles for treatment of this disease. Nonetheless, RT should have no role in preventing multifocal tumorigenesis, which will be continuously encountered by multidisciplinary approaches (21).

The risk of developing serious gastrointestinal sequela after PRT is another important issue to consider in patients who have HCC located adjacent to the digestive tract. We attempted once-daily fractionation of PRT with 65 CGE/26 fractions. However, 2 of 11 patients who received this treatment developed gastrointestinal toxicity grade of ≥2. Moreover, these 11 patients showed significantly worse LPF rates than those who received 76 CGE/20 fractions of PRT. Three patients who received 60 CGE/10 fractions of PRT were controlled locally. Although our current data are based on a limited number of patients, precluding definitive conclusions, they suggest a low α/β ratio (22) of HCC, and this assumption should be examined further in clinical trials. Based on currently available data, efforts to exclude the gastrointestinal loop from the PTV by using, for example, surgical manipulations, seem to be positively considered in order to expand the role of PRT for HCC.

CONCLUSIONS

In conclusion, PRT achieved excellent local progression-free rates when aggressive, high-dose/fractionation was administered. Child-Pugh class A patients with ICG R15 of less than 40% tolerated PRT of a large irradiated volume well, despite development of transient PHI. However, in Child-Pugh class B patients, it seems reasonable to minimize the irradiated volume to prevent detrimental liver damage induced by PRT and underlying liver diseases. A V30 of less than 25% in the noncancerous portion of the liver is considered an indicator of the safety of PRT in patients who have pre-PRT ICG R15 of 20% to 50%. We believe that there are extremely few indications for PRT in patients who have ICG R15 of 50% or higher. Gastrointestinal toxicity is a major drawback of PRT for tumors adjacent to the gastrointestinal tract, and surgical manipulation to exclude the intestinal loop from the PTV should be positively considered as indicated. If these issues are carefully considered, with special attention to the patterns of tumor spread, when determining the

CTV, aggressive high-dose PRT could become a legitimate treatment for a certain population of patients with unresectable HCC for whom there is no standard treatment available other than TACE or liver transplantation.

REFERENCES

1. Krishnan S, Dawson LA, Seong J, *et al.* Radiotherapy for hepatocellular carcinoma: An overview. *Ann Surg Oncol* 2008;15: 1015–1024.
2. Bush DA, Hillebrand DJ, Slater JM, *et al.* High-dose proton beam radiotherapy of hepatocellular carcinoma: Preliminary results of a phase II trial. *Gastroenterology* 2004;127:S189–S193.
3. Kawashima M, Furuse J, Nishio T, *et al.* Phase II trial of radiotherapy employing proton beam for hepatocellular carcinoma. *J Clin Oncol* 2005;23:1839–1846.
4. Chiba T, Tokuuye K, Matsuzaki Y, *et al.* Proton beam therapy for hepatocellular carcinoma: A retrospective review of 162 patients. *Clin Cancer Res* 2005;11:3799–3805.
5. Kosuge T, Makuuchi M, Takayama T, *et al.* Long term results after resection of hepatocellular carcinoma: experience of 480 cases. *Hepato-Gastroenterol* 1993;40:328–332.
6. The Liver Cancer Study Group of Japan. Predictive factors for long term prognosis after partial hepatectomy for patients with hepatocellular carcinoma in Japan. *Cancer* 1994;74:2772–2780.
7. Makuuchi M, Sano K. The surgical approach to HCC: Our progress and results in Japan. *Liver Transpl* 2004;10:S46–S52.
8. Tsai TJ, Chau GY, Lui WY, *et al.* Clinical significance of microscopic tumor venous invasion in patients with resectable hepatocellular carcinoma. *Surgery* 2000;127:603–608.
9. Vauthey JN, Lauwers GY, Esnaola NF, *et al.* Simplified staging for hepatocellular carcinoma. *J Clin Oncol* 2002;20:1527–1536.
10. Imamura H, Sano K, Sugawara Y, Kokudo N, Makuuchi M. Assessment of hepatic reserve for indication of hepatic resection: Decision tree incorporating indocyanine green test. *J Hepatobiliary Pancreat Surg* 2005;12:16–22.
11. Esnaola NF, Lauwers GY, Mirza NQ, *et al.* Predictors of microvascular invasion in patients with hepatocellular carcinoma who are candidates for orthotopic liver transplantation. *J Gastrointest Surg* 2002;6:224–232.
12. Cammà C, Schepis F, Orlando A, *et al.* Transarterial chemoembolization for unresectable hepatocellular carcinoma: Meta-analysis of randomized controlled trials. *Radiology* 2002;224: 47–54.
13. Takayasu K, Arii S, Ikai I, *et al.* Prospective cohort study of transarterial chemoembolization for unresectable hepatocellular carcinoma in 8510 patients. *Gastroenterology* 2006;131: 461–469.
14. Lawrence TS, Tesser RJ, Ten Haken RK. An application of dose volume histograms to the treatment of intrahepatic malignancies with radiation therapy. *Int J Radiat Oncol Biol Phys* 1990;19:1041–1047.
15. Tsujii H, Tsuji H, Inada T, *et al.* Clinical results of fractionated proton therapy. *Int J Radiat Oncol Biol Phys* 1993;25:49–60.
16. Ando K, Furusawa Y, Suzuki M, *et al.* Relative biological effectiveness of the 235 MeV proton beams at the National Cancer Center Hospital East. *J Radiat Res* 2001;42:79–89.
17. Schwartz JD, Schwartz M, Mandeli J, Sung M. Neoadjuvant and adjuvant therapy for resectable hepatocellular carcinoma: review of the randomised clinical trials. *Lancet Oncol* 2002;3: 593–603.
18. Méndez Romero A, Wunderink W, Hussain SM, *et al.* Stereotactic body radiation therapy for primary and metastatic liver tumors: A single institution phase I-II study. *Acta Oncol* 2006;45: 831–837.
19. Choi BO, Jang HS, Kang KM, *et al.* Fractionated stereotactic body radiotherapy in patients with primary hepatocellular carcinoma. *Jpn J Clin Oncol* 2006;36:154–158.
20. Liang SX, Zhu XD, Lu HJ, *et al.* Hypofractionated three-dimensional conformal radiation therapy for primary liver carcinoma. *Cancer* 2005;103:2181–2188.
21. Avila MA, Berasain C, Sangro B, Prieto J. New therapies for hepatocellular carcinoma. *Oncogene* 2006;25:3866–3884.
22. Thames HD, Withers HR, Peters LJ, *et al.* Changes in early and late radiation responses with altered dose fractionation: Implications for dose-survival relationships. *Int J Radiat Oncol Biol Phys* 1982;8:219–226.

JOURNAL OF APPLIED CLINICAL MEDICAL PHYSICS, VOLUME 12, NUMBER 2, SPRING 2011

Proton dose distribution measurements using a MOSFET detector with a simple dose-weighted correction method for LET effects

Ryosuke Kohno,[1,2a] Kenji Hotta,[3,4] Taeko Matsuura,[5] Kana Matsubara,[6] Shie Nishioka,[1,7] Teiji Nishio,[1] Mitsuhiko Kawashima,[1] Takashi Ogino,[1]
National Cancer Center Hospital East,[1] Chiba 277-8577, Japan; National Cancer Center Research Institute,[2] Tokyo 104-0045, Japan; Pure and Applied Sciences,[3] University of Tsukuba, Tsukuba, Ibaraki 305-8577, Japan; Research Fellow of the Japan Society for the Promotion of Science;[4] Department of Medical Physics,[5] Hokkaido University Hospital, Hokkaido 060-8648, Japan; Graduate School of Human Health Sciences,[6] Tokyo Metropolitan University, Tokyo 116-8551, Japan; Foundation for Promotion of Cancer Research,[7] Tokyo, 104-0045, Japan.
rkohno@east.ncc.go.jp

Received 16 August, 2010; accepted 7 January, 2011

We experimentally evaluated the proton beam dose reproducibility, sensitivity, angular dependence and depth-dose relationships for a new Metal Oxide Semiconductor Field Effect Transistor (MOSFET) detector. The detector was fabricated with a thinner oxide layer and was operated at high-bias voltages. In order to accurately measure dose distributions, we developed a practical method for correcting the MOSFET response to proton beams. The detector was tested by examining lateral dose profiles formed by protons passing through an L-shaped bolus. The dose reproducibility, angular dependence and depth-dose response were evaluated using a 190 MeV proton beam. Depth-output curves produced using the MOSFET detectors were compared with results obtained using an ionization chamber (IC). Since accurate measurements of proton dose distribution require correction for LET effects, we developed a simple dose-weighted correction method. The correction factors were determined as a function of proton penetration depth, or residual range. The residual proton range at each measurement point was calculated using the pencil beam algorithm. Lateral measurements in a phantom were obtained for pristine and SOBP beams. The reproducibility of the MOSFET detector was within 2%, and the angular dependence was less than 9%. The detector exhibited a good response at the Bragg peak (0.74 relative to the IC detector). For dose distributions resulting from protons passing through an L-shaped bolus, the corrected MOSFET dose agreed well with the IC results. Absolute proton dosimetry can be performed using MOSFET detectors to a precision of about 3% (1 sigma). A thinner oxide layer thickness improved the LET in proton dosimetry. By employing correction methods for LET dependence, it is possible to measure absolute proton dose using MOSFET detectors.

PACS number: 87.56.-v

Key words: proton, MOSFET detector, LET, simple dose-weighted correction method, *in vivo* dosimetry

I. INTRODUCTION

The Metal Oxide Semiconductor Field Effect Transistor (MOSFET) detector is widely used as a pinpoint dosimeter for photon and electron dose verification.[1-6] The typical design uses

[a] Corresponding author: Ryosuke Kohno, National Cancer Center Hospital East, 6-5-1 Kashiwanoha, Kashiwa-shi, Chiba 277-8577, Japan; phone: +81-4-7133-1111; fax: +81-4-7134-7048; email: rkohno@east.ncc.go.jp

a p-channel enhanced MOSFET constructed on a negatively doped (n-type) silicon substrate. Ionizing radiation generates electron-hole pairs in the insulating layer. The holes drift toward the substrate under an appropriate bias voltage and are semipermanently trapped at the interface, resulting in a shift in the gate voltage required for source-drain conductivity that is proportional to the radiation dose. Following exposure, the gate threshold voltage is measured by applying a constant source-drain current, and the cumulative dose is obtained using suitable calibration factors. The major advantages of this detector include small physical size, the ability to permanently store the accumulated dose, dose-rate and temperature independence, real-time readout, roughly isotropic response for photon beams, and ease of use.

Kohno et al.[7] evaluated the use of the commercially available TN-502RD MOSFET detector with oxide thicknesses of 0.5 μm (Best Medical Canada, Ottawa, Canada) for proton dose measurement. The dose reproducibility, linearity, fading effect and beam intensity dependence were similar to the response obtained from photon beams. On the other hand, Bragg curves measured using the TN-502RD at high bias settings were 20%–40% lower than those measured using an ionization chamber. The MOSFET response is strongly dependent on the degree of linear energy transfer (LET) occurring through columnar recombination. This is due to the significant reduction in charge recombination when the electric field applied to the MOSFET is perpendicular to the plasma track, leading to faster drift of electron-hole pairs. As a result of the LET dependence and the columnar recombination effect, quantitative proton dose measurements are difficult to accurately perform using MOSFET detectors. In order to use a MOSFET detector for proton dosimetry, improved characterization of the response in the Bragg peak region is necessary. Kohno et al.[7] also reported that the response of the TN-502RD was approximately 15% higher than the IC detector at most angles. A lower angular dependence would be desirable when using MOSFET detectors for *in vivo* proton dosimetry.

Cheng et al.[8] investigated another OneDose single use MOSFET detector (Sicel Technologies, Inc., Morrisville, NC) for *in vivo* dosimetry in proton beam therapy. The OneDose detector generally underresponsed compared to the Markus chamber, about 5% at depth of ~ 5 cm, and increase to ≤ 200% at the Bragg peak and beyond. Although it is difficult to measure the Bragg peak with the OneDose, the Cheng study reported that the OneDose provides an opportunity to measure surface dose with proton beam within acceptable clinical criterion of ± 5.0%–6.5%.

In this study, we examined a new MOSFET detector with an oxide thickness of 0.25 μm (TN-252RD) to improve characterization of the MOSFET response for proton beams. The dose sensitivity, angular dependence, and depth-dose response were experimentally evaluated at high bias settings using a 190 MeV proton beam. We also implemented a simple dose-weighted correction method to account for LET dependence suitable for clinical applications. This method was used to perform absolute proton dosimetry using the MOSFET detector.

II. MATERIALS AND METHODS

A. MOSFET dosimetry system

A commercially available MOSFET patient dose verification system (Best Medical Canada, Ottawa, Canada) was used. In order to reduce temperature dependence and nonlinear response at high-dose levels,[9] the dual-MOSFET is composed of two identical MOSFETs, fabricated on the same silicon substrate, with an active area of 0.2×0.2 mm^2. This placement allows for temperature compensation as the two MOSFETs are located on the same substrate. The oxide thickness for the TN-252RD MOSFET is 0.25 μm. The detectors are $2 \times 1.3 \times 8$ mm in size including the encapsulation.[10] All measurements were performed using a high-sensitivity bias voltage setting.

B. Experimental apparatus

B.1 Proton beam setup

Measurements were carried out using the therapeutic proton beam line at the National Cancer Center Hospital East, Japan. The beam line employs the dual-ring double-scattering method for proton therapy.[11] The thickness of the first scatter and the shape of the second scatter are determined by the energy of the proton beams. The maximum size of the irradiation field provided by this system is 200 mm in diameter. The energy of the proton beam was maintained at 190 MeV, and daily testing was used to ensure the proton range was within ± 0.5 mm.[12]

B.2 MOSFET sensitivity and dose calibration

In MOSFET sensitivity (mV/cGy) measurements, the proton energy was 157 MeV at a detector located within a PMMA dose calibration phantom. At this energy the MOSFET detectors displayed no response changes due to LET dependence. A calibrated 0.6 cc Farmer ionization chamber (IC) type 30013 (PTW, Freiburg, Germany) and MOSFET detector were placed along a line perpendicular to the beam axis. The MOSFET and the IC were exposed five times to 200 cGy, and the MOSFET sensitivity was determined from the average output. The sensitivity of the MOSFET detector was also measured using proton beams with energies of 50, 100, 150, 157 and 200 MeV.

For accurate comparisons, the detector outputs were converted to dose values. The dose calibration factor (F_{calib}) in cGy/mV for the MOSFET detector was measured using a 157 MeV proton beam. The raw dose (D_{raw}) for the MOSFET detector was obtained from the product of the MOSFET reading R in mV and the dose calibration factor:

$$D_{raw} = F_{calib} \times R \tag{1}$$

B.3 Angular dependence

The response of MOSFET detectors is dependent on the angle of incidence.[1-5,7] The angular dependence was experimentally evaluated using a cylindrical acrylic phantom with a radius of 8 cm and a length of 15 cm. The angular response with respect to the cable axis was measured at 30°, 45°, 60°, 90°, 120°, 135°, 150°, and 180°.

B.4 Depth-dose curves

Depth-dose curves for mono-energetic proton beams were determined using the IC and MOSFET detectors. Polyethylene (PE) slabs ranging in thickness from 0 to 175 mm were stacked on top of the calibration phantom containing the detectors. The equivalent water thickness was calculated by multiplying the polyethylene thickness by 1.02. The measurements were repeated three times at each thickness, and the results were normalized with respect to the response at a thickness of 0 mm. The ratio of the response of the IC detector to the MOSFET detector was also plotted as a function of thickness. The correction factors (IC/MOSFET) were expressed as a function of the PE thickness (d_{PE}): $cf_{mono}(d_{PE})$.

In actual proton therapy, most patients are treated using a SOBP proton beam created using a ridge-filter. We therefore also measured the depth-dose distribution of an 80 mm SOBP-width proton beam using the MOSFET detector. The ratio of the IC response to the MOSFET response (IC/MOSFET) was obtained and the correction factor cf_{SOBP} was determined as a function of d_{PE} as was done for the mono-energetic proton beam.

C. Dose distribution formed by the protons traversing an L-shaped bolus

C.1 Experimental apparatus

We prepared a polyethylene bolus with an L-shaped horizontal cross section (Fig. 1). The bolus was 50 mm thick at points where $x < 0$ and 10 mm thick when $x \geq 0$. This bolus shape was selected to correspond to the target with large heterogeneity in the lateral direction. Particularly,

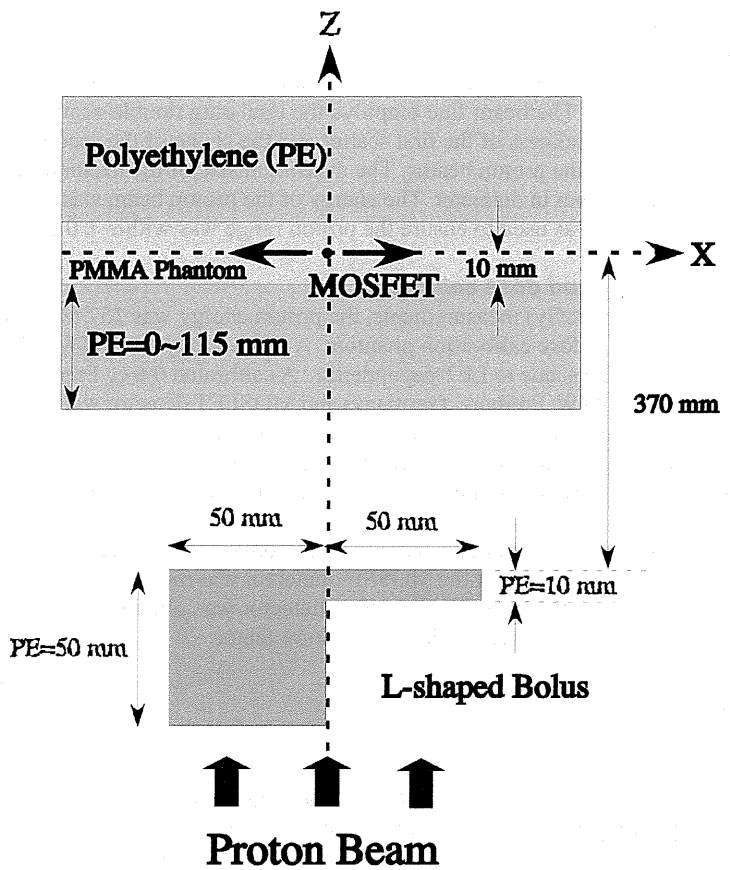

FIG. 1. Experimental arrangement for measurement of dose distribution (top view). The bolus was made of polyethylene.

we expect lateral dose distributions around x = 0 form a complex bump and dip structure due to the bolus edge scattering effect of the bolus region where the thickness changes abruptly. The correction factor of the MOSFET response must take these effects into consideration.

For the 190 MeV mono-energetic proton beam, the Bragg peak positions were 110 mm for protons passing through the thicker section and 150 mm for protons passing through the thinner section. Polyethylene slabs of various thicknesses were stacked on top of the PMMA calibration phantom. The lateral (x-axis) dose distributions were measured using the IC and the TN-252RD MOSFET detector at PE thicknesses of 0, 100, 105, 110 and 115 mm. In addition, we measured the lateral dose distributions at PE thicknesses of 0, 50 and 100 mm for the 80 mm SOBP-width beam.

C.2 A simple dose-weighted correction method

Because of LET dependence, there is a notable disagreement between the IC and the TN-502RD MOSFET detector near the Bragg peak.[7] Knowledge of the LET spectrum is important in cavity theory to account for recombination effects and stopping power ratios.[13] The difference in response cannot be completely explained by differences in stopping power between water and SiO_2. In addition, proton beam therapy uses a spread-out Bragg peak (SOBP) beam containing protons with a range of energies, making it difficult to easily and accurately calculate the LET spectrum at a particular measurement point due to bolus and tissue heterogeneities.

In order to provide a simple correction for the response of the MOSFET detector to various LET effects, we employed a method originally used to correct imaging plate response.[14] A Bragg curve was obtained using the IC detector to establish a standard for the proton beam depth-dose distribution. This curve was then used to calculate correction factors (IC/MOSFET) as a function of proton penetration depth.

The proton penetration depth can be considered as a residual range. Since the protons at any point have a variety of energies due to multiple scattering effects, the residual proton range at an arbitrary point may be calculated using the pencil beam dose calculation algorithm (PBA),[15-17] in which the pencil beam dose distribution is separated into a central-axis term and an off-axis term. The central-axis term represents the measured depth-dose distribution of the broad beam. The off-axis term is a two-dimensional Gaussian distribution the standard deviation of which corresponds to the lateral beam spread. The dose $F(x, y, z, (x_0, y_0))$ delivered by a single pencil beam at an entrance position (x_0, y_0) is given by:

$$F(x,y,z;(x_0,y_0)) = \phi(x_0,y_0)DD(z;(x_0,y_0)) \times \frac{1}{2\pi\sigma(z)^2}\exp\left(-\frac{(x_0-x)^2-(y_0-y)^2}{2\sigma(z)^2}\right), \quad (2)$$

where $\phi(x_0,y_0)$ is the intensity profile of the broad beam, $DD(z;(x_0,y_0))$ is the depth-dose distribution of the broad beam, and $\sigma(z)$ is the proton spread due to multiple scattering effects in the bolus and polyethylene slabs and the configuration of the beam line at z. We can obtain the dose distribution in the region of interest by generating many pencil beams and summing their dose distributions. For dose distributions of protons traversing an L-shaped phantom, Kohno et al.[16] reported the precision of doses calculated using the PBA is approximately 2.5%. The PBA may therefore be considered a precise and practical method for calculating the proton residual range in order to obtain correction factors at arbitrary locations.

The correction factor for the MOSFET response CF(x,y,z) is given by:

$$CF(x,y,z) = \frac{\sum_{i=1}^{n} cf_{dd}(z;(x_i,y_i))F(x,y,z;(x_i,y_i))}{\sum_{i=1}^{n} F(x,y,z;(x_i,y_i))} \quad (3)$$

in which i is the ith pencil beam, n is the total number of pencil beams, (x_i,y_i) is the position of a generated pencil beam, and $cf_{dd}(z;(x_i,y_i))$ is $cf_{mono}(z = d_{PE})$ or $cf_{SOBP}(z = d_{PE})$ (as described in Section B.4 above). The dose measured by the MOSFET detector at (x,y,z), D(x,y,z) may be calculated using:

$$D(x,y,z) = CF(x,y,z) \cdot D_{raw}(x,y,z), \quad (4)$$

where $D_{raw}(x,y,z)$ is the raw dose (as described in Section B.2 above).

Proton dose distributions resulting from an L-shaped bolus (Fig. 1) were measured using the MOSFET and the IC detectors. Protons passing near the abrupt change in thickness at x = 0 displayed a range of energies due to multiple scattering effects, and it was necessary to calculate the proton residual range using the PBA in order to obtain the correction factor.

III. RESULTS & DISCUSSION

A. Dose sensitivity

The sensitivity of the TN-252RD MOSFET detector was 0.72 ± 0.01 (mV/cGy) and the corresponding reproducibility was ± 1.4%. Although the sensitivity of this detector was lower than the TN-502RD MOSFET with a thicker oxide layer, its reproducibility was within 2%. Figure 2 is a graph of the TN-252RD MOSFET sensitivity for each proton energy value. The sensitivities to 150, 157, and 200 MeV proton beams were almost identical, but the sensitivity was reduced at lower proton energies of 100 and 50 MeV.

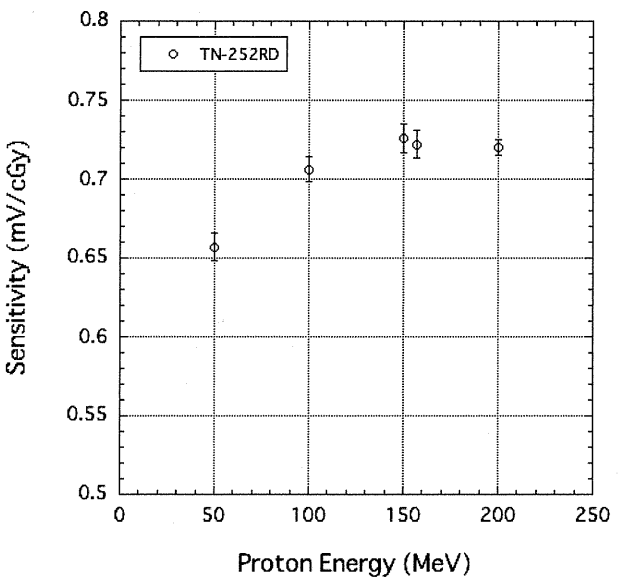

FIG. 2. MOSFET sensitivity for 200, 157, 150, 100 and 50 MeV proton beams.

B. Angular dependence

Figure 3 depicts an angular dependence of the MOSFET detector exposed to a 190 MeV proton beam, and the correction value for the angular response of the MOSFET detector. The electric field is parallel to the incident proton beam when the MOSFET detector is mounted at 0 degrees. The response was normalized to 0°, corresponding to a beam perpendicular to the MOSFET encapsulation epoxy. The angular response at 180° agreed well with the 0° measurements (within ± 2.0%). The TN-252RD detector displayed a maximum overresponse of +9.0%. The overresponse occurs because the fraction of charge pairs escaping recombination increases at larger angles between the electric field and the proton track.[18] Despite the large value, this is a dramatic improvement of almost 10% relative to the TN-502RD device,[7] suggesting that MOSFET detectors constructed using thinner SiO_2 layers exhibit reduced angular dependence. The correction value $CV_{Ang}(\theta)$ may be obtained from the angular response of the TN-252RD detector at a beam angle θ using the relation:

$$CV_{Ang}(\theta) = 1 - 0.00197 \cdot \theta + 0.0000109 \cdot \theta^2. \quad (5)$$

Using this correction value, we can correct the angular response of the TN-252RD MOSFET detector to within 1.5%.

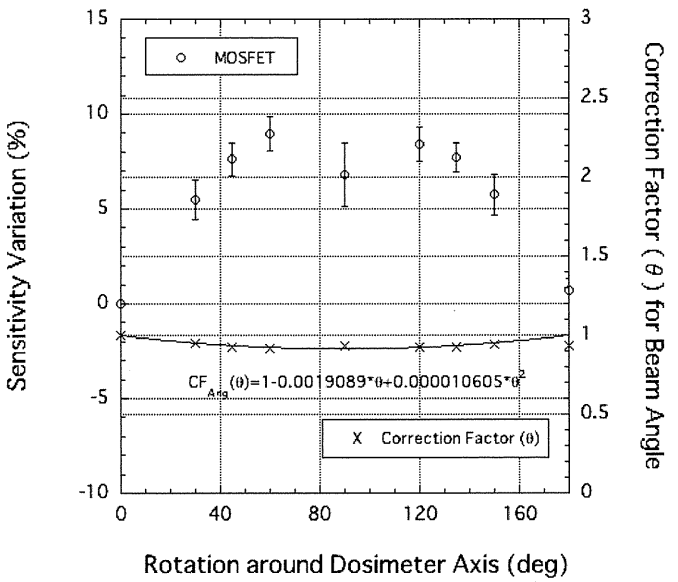

FIG. 3. Angular dependence of MOSFET detectors exposed to a 190 MeV proton beam. The correction value for the angular response of the MOSFET detector is also plotted.

C. Depth-dose curves

Figure 4 shows a comparison of Bragg curves obtained using IC and MOSFET detectors at high-bias setting for a 190 MeV proton beam, and the correction factor for the response of the MOSFET detector was calculated as a function of proton penetration depth. The relative response of the TN-252RD MOSFET detector at the Bragg peak was 0.74. This response relative to the TN-502RD detector[7] also is a larger than a 10% improvement. The correction factor $cf_{mono}(z = d_{PE})$ for the response of the MOSFET detector was determined as a function of proton penetration depth as follows:

$$cf_{mono}(d_{PE}) = \begin{cases} 1 & [d_{PE} < 100.421\,(mm)] \\ 0.781885 + 0.002172 \cdot d_{PE} & [100.421\,(mm) \le d_{PE} < 154.784\,(mm)] \\ -2.94139 + 0.0262266 \cdot d_{PE} & [154.784\,(mm) \le d_{PE}] \end{cases} \quad (6)$$

The MOSFET with the correction agreed well with the IC within 1.5%, as shown in Fig. 4.

A comparison of the SOBP obtained using the IC and MOSFET detectors is shown in Fig. 5. Figure 5 also shows the correction factor for the response of the MOSFET detector was calculated as a function of proton penetration depth. The ratio of the IC and MOSFET (IC/MOSFET) response was also obtained. The correction factor $cf_{SOBP}(d_{PE})$ was expressed as a function of PE thickness using:

$$cf_{SOBP}(d_{PE}) = \begin{cases} 1 & [d_{PE} < 40\,(mm)] \\ 0.94639 + 0.00134025 \cdot d_{PE} & [40\,(mm) \le d_{PE} < 140\,(mm)] \\ 6.59257 - 0.0793194 \cdot d_{PE} + 0.00028807 \cdot d_{PE}^{\,2} & [140\,(mm) \le d_{PE}] \end{cases} \quad (7)$$

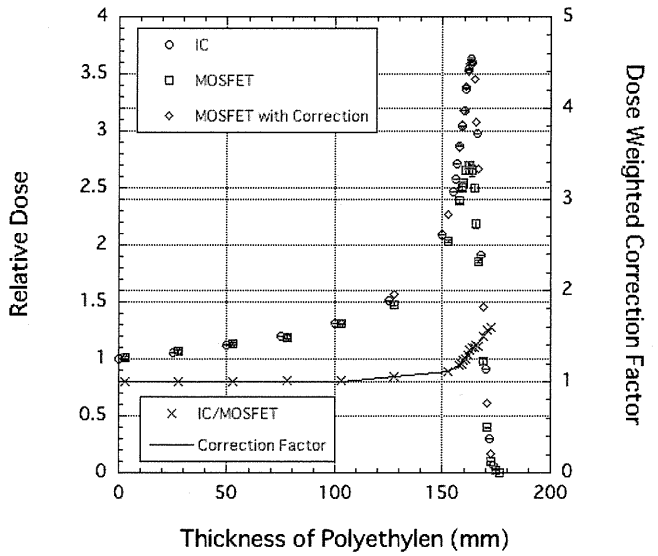

FIG. 4. Comparison of Bragg curves obtained using IC and MOSFET detectors at high-bias setting for a 190 MeV proton beam. The correction factor for the response of the MOSFET detector was calculated as a function of proton penetration depth.

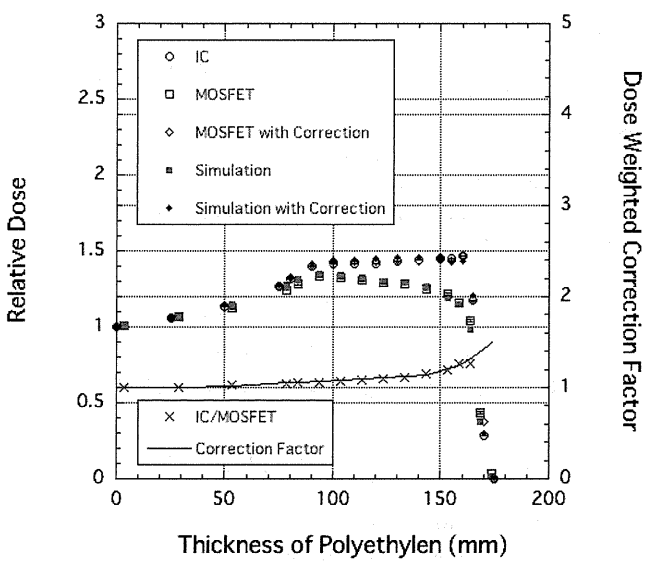

FIG. 5. Comparison of SOBP obtained using IC and MOSFET detectors. The correction factor for the response of the MOSFET detector was calculated as a function of proton penetration depth.

The MOSFET with the correction agreed well with the IC within 1.4%, as shown in Fig. 5.

In this method, $cf_{SOBP}(d_{PE})$ must be measured and calculated for each SOBP width. However, a SOBP distribution may be obtained in a stepwise manner from the dose contributions of mono-energetic proton beams traversing the individual elements of the ridge filter. For example, the "Simulation" curve in Fig. 5 depicts the SOBP distribution obtained using the

uncorrected depth-output curve measured with the MOSFET detector. The "Simulation with Correction" curve depicts results corrected without the necessity of applying the experimentally determined MOSFET response corrections to the "Simulation" curve. Thus, given $cf_{mono}(d_{PE})$ of Eq. (6) for the mono-energetic proton beam, we can obtain $cf_{SOBP}(d_{PE})$ for various SOBP-width proton beams by simulating the SOBP beam using the Bragg curve of a mono-energetic proton beam.

D. Bolus experiments

Figure 6 compares the lateral dose distributions obtained for a 190 MeV proton beam using IC and MOSFET detectors at PE thicknesses of 0 (a), 100 (b), 105 (c), 110 (d) and 115 (e) mm. The error bar in Fig. 6 includes the reproducibility of the MOSFET measurements and calculation errors of 3% to account for uncertainties in the PBA (as described in Materials and Methods Section C.2). In Fig. 6(a), a bump and dip structure is evident near x = 0. This is the result of edge scattering effects due to the abrupt change in thickness. The uncorrected MOSFET results agreed well with the IC measurements, and the MOSFET response due to LET did not change at this depth. Thus, in shallow regions, depth-dose distribution corrections are unnecessary.

On the other hand, the MOSFET detector response began to change at $x < 0$ and the uncorrected MOSFET output deviated significantly from the IC response (Fig. 6(b)). Because the depth at $x < 0$ is close to the Bragg peak position, the MOSFET response was reduced. Since edge scattering causes the lateral dose distribution near x = 0 to be determined by protons with a distribution of energies, we expected that changes in the MOSFET response would be complex. However, the corrected output of the MOSFET detector agreed well with the IC results within an average difference of 4.4%, demonstrating that MOSFET detectors are suitable for proton dosimetry when the response is corrected. Despite the drastic change in MOSFET detector response near $x < 0$ for PE thicknesses of 105, 110 and 115 mm, the corrected output agreed with the IC results (Figs. 6(c), 6(d), and 6(e)) within 3.2% (1 sigma).

Figure 7 is a comparison of the lateral-dose distribution obtained using the IC and MOSFET detectors at PE thicknesses of 0 (a), 50 (b) and 100 (c) mm for an SOBP proton beam. The corrected MOSFET output agreed well with the IC results. For the SOBP beam, the accuracy of the dose measurement was approximately 2.3% (1 sigma).

By employing correction methods for LET and angular dependence, it is possible to perform *in vivo* proton dosimetry using a MOSFET detector. However, the correction method for LET effects is highly dependent on the precision of the PBA calculation, and further improvements to the dose calculation algorithm (for instance the application of Monte Carlo methods) would be desirable in situations involving tissues with significant heterogeneity.[19-23]

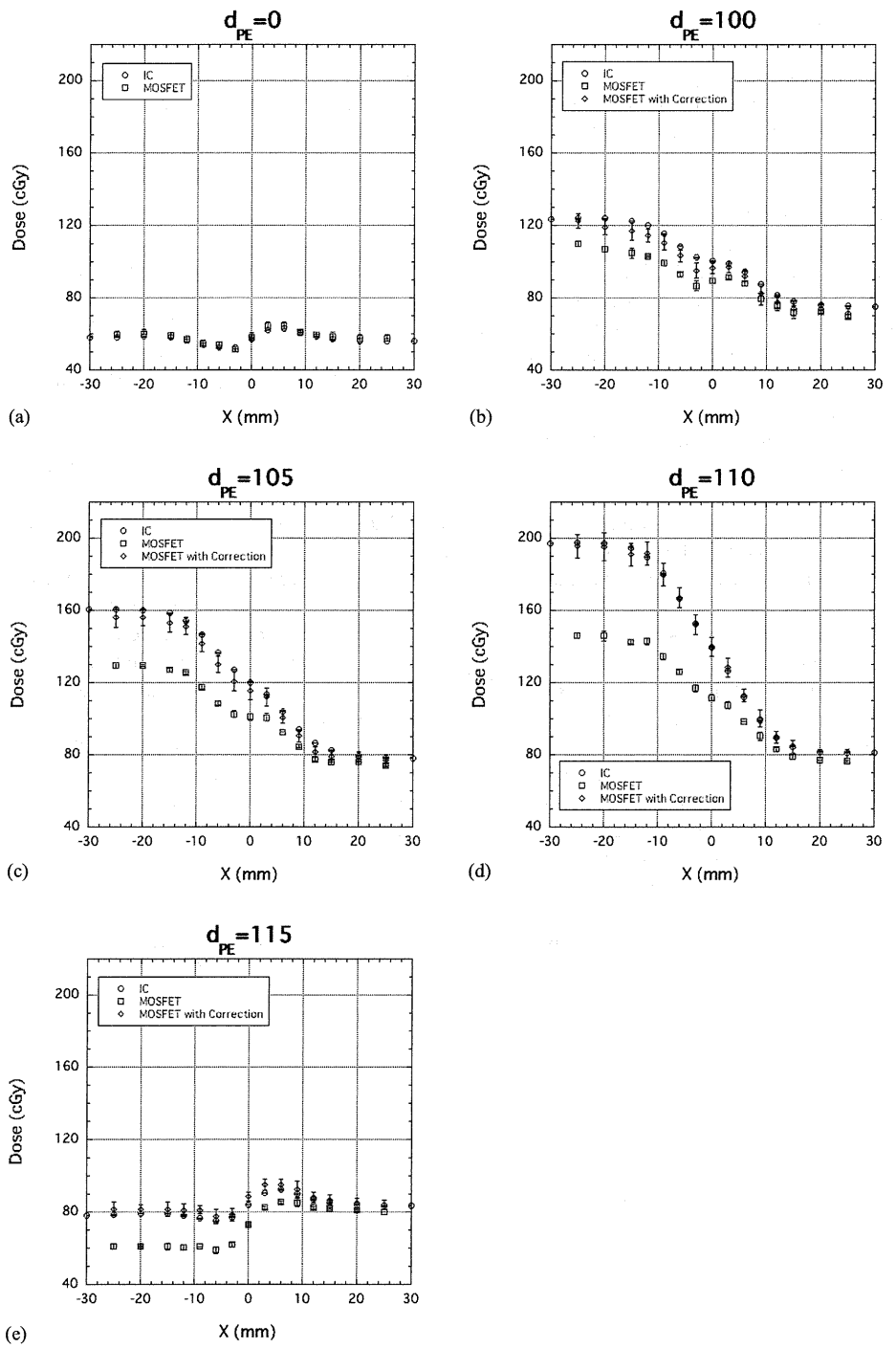

FIG. 6. Comparison of lateral-dose distribution obtained using IC, uncorrected MOSFET (MOSFET) and corrected MOSFET detectors (MOSFET with Correction) at PE thicknesses of 0 (a), 100 (b), 105 (c), 110 (d) and 115 (e) mm for a 190 MeV mono-energetic proton beam.